ACS APPLIED MATERIALS & INTERFACES

www.acsami.org

Research Article

Multiscale Simulation of Solid Electrolyte Interface Formation in Fluorinated Diluted Electrolytes with Lithium Anodes

Peiping Yu,[†] Qintao Sun,[†] Yue Liu, Bingyun Ma, Hao Yang, Miao Xie, and Tao Cheng*

Cite This: *ACS Appl. Mater. Interfaces* 2022, 14, 7972–7979

Read Online

ACCESS | Metrics & More | Article Recommendations | Supporting Information

ABSTRACT: Lithium metal batteries (LMBs) hold great promise in facilitating high-energy batteries due to their merits such as high specific capacity, low reduction potential, and so forth. However, the realizations of practical LMBs are hindered by severe problems such as undesirable dendrite growth, poor Coulombic efficiency, and so forth. A recently proposed fluorinated electrolyte based on 1 M lithium bis(fluorosulfonyl)imide (LiFSI) dissolved in designed fluorinated 1,4-dimethoxybutane (FDMB) solvent has attracted significant attention because of its excellent electrochemical performance that origins from its superior physical and chemical properties, especially its unique ability in forming a robust, stable solid electrolyte interphase (SEI). However, the detailed structure and reaction mechanism of the SEI formation in such a novel electrolyte remains unclear. In this work, we carry out a hybrid *ab initio* and reactive molecular dynamics (HAIR) simulation to investigate the elementary reactions that regulate the formation of the primitive SEI, paying special attention to the process that involves FDMB, the fluorinated solvent. HAIR simulation reveals that both FSI^- anion and FDMB provide F that is adequate to form a uniformed LiF layer that resembles the inorganic inner layer (IIL) of the SEI. N and S radicals from the FSI^- anion, which do not deposit on the electrode interface to form lithium-containing inorganic substances, promote the polymerization reaction of unsaturated carbon chains produced by FDMB defluorination, forming the organic outer layer (OOL) of the SEI. The combination of the LiF-rich IIL and polymer-rich organic OOL explains the superior performance of the FDMB-based electrolyte in the device. The detailed reaction mechanism and SEI observed in this work provide insights into the atomic scale for the rational design of F-rich electrolytes in the near future.

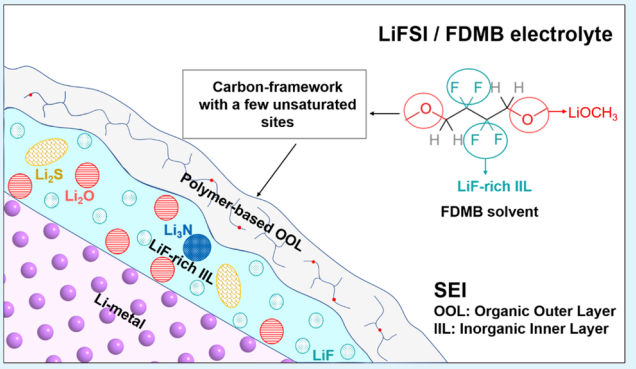

KEYWORDS: *lithium metal battery, density functional theory, reactive force field, ab initio molecular dynamics, local high concentration electrolyte*

1. INTRODUCTION

Lithium (Li)-ion batteries (LIBs) have emerged as one of the most effective electrochemical energy storage devices in the last 3 decades, radically reshaping our daily lives. Long cycle life, high energy efficiency, high energy density, minimal self-discharge, and other merits grant LIBs' success in applications such as the portable device, electric vehicles (EV) to the energy grid, and so forth. As the manufacturing process improves, the energy density of the state-of-art LIBs is approaching its theoretical limit (372 mA h/g). However, batteries with higher energy density are required to meet the emerging EV market and the surging demand for grid energy storage. As a result, there is a renewed interest in rechargeable Li metal batteries, with a theoretical capacity of 3860 mA h/g, in the scientific and industrial worlds [lithium metal batteries (LMBs)].[1−5]

Nevertheless, the application of LMBs is significantly impeded by challenging problems such as uncontrollable side reactions between the lithium metal anode and electrolyte, unexpected lithium dendrite growth, and so forth. The solid electrolyte interphase (SEI) is an interface that spontaneously forms between the electrolyte and anode due to the mismatch between the electrode potential and electrolyte electrochemical window.[6,7] An ideal SEI should be electronically insulated and chemically inert to prevent irreversible side reactions between electrolytes and lithium metals, while allowing for fast ion conduction. It has been demonstrated by previous research that a robust, passivated SEI can efficiently protect the Li anode from facilitating high Coulombic efficiency (CE) in numerous cycles, which can be achieved via rational electrolyte design.

Received: November 21, 2021
Accepted: January 21, 2022
Published: February 7, 2022

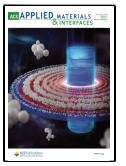

Over the past few years, a significant amount of experiments have demonstrated that the structure and performance of the SEI can be finely tuned by methods, such as salt additive optimization, solvent ratio modification, and liquefied gas electrolytes. In particular, high-concentration electrolytes (HCEs) and localized high-concentration electrolytes (LHCEs) have been recognized to be one of the most effective methods. For example, Yamada *et al.*[8] designed a series of HCEs that can resist high oxidation voltage and exhibit excellent cycling performance, while maintaining high CE over the whole range of applied voltages (U). The authors also found that as the interaction between cations and anions/solvents increased, the ratio of free solvents significantly decreased as the salt concentration increased, as revealed from the density functional theory−molecular dynamics (DFT-MD) simulation. Such change is of help in avoiding electrolyte volatilization and the side reactions with the cathode, explaining the superior performance.[9] In addition, HCEs with unique 3D solution structures promote the decomposition of salt anions, which sacrificially protect the solvent and release enough F^- to form LiF, an inorganic component, deemed to be beneficial to promise appreciate mechanical and chemical properties that guarantee superior performance.[8−14] Despite their advantage in improving the performance, HCEs have their inherent problems, including high costs, high viscosity, and so forth, which greatly limit its large-scale commercialization. Although the LHCEs have been proposed and realized to solve the abovementioned problems by adding less expensive diluents, problems, such as low Li^+ solubility, still exist.[11,15,16]

Improving battery performance by adjusting the salt-to-solvent ratio appears to have hit a limit, and a new type of solvent may be able to balance the performance and cost concerns of LMB systems. Because ethers are stable with lithium, they are frequently utilized as electrolytes in lithium batteries.[10,17−20] However, organic solvent decomposition is the most common way to generate free H radicals that likely leads to the thermal runaway. One way to suppress such a safety problem is to replace H of ether electrolyte with F; inherency reduces H formation, thereby reducing the risk of the electrolyte.[12,21−23] Therefore, fluoride solvent-based liquid electrolytes are a promising candidate to prevent combustion or exploration in designing safe batteries.[24] Moreover, fluorinated solvent also provides F^- to form a high-quality SEI by forming rich in LiF, which helps regulate lithium electrodeposition behavior and inhibits lithium dendrite formation.[25−28]

Recently, a new electrolyte design strategy has been proposed by Yu *et al.*, which introduces a $-CF_2-CF_2-$ unit into the DME solvent to facilitate fluorinated 1,4-dimethoxybutane (FDMB).[29] This solvent is stable with the Li metal and can increase Li^+ solubility. The authors composed this solvent and salt LiFSI into a 1 M LiFSI/FDMB single salt and single solvent electrolyte, which showed a high(>6 V) oxidation voltage and high cycle CE (>99.98%, 420 cycles). The ultrathin SEI with only ∼6 nm thickness was observed in Cryo-TEM, which effectively separated the Li anode and electrolyte.

Despite the fact that producing enhanced electrolytes with higher performance is a new method in LMB, the decomposition mechanism of this novel solvent FDMB and its impact on the SEI formation process are still unclear. Theoretical modeling has been widely employed to reveal the atomic details of reactions in the battery.[6,30−34] Previous theoretical studies have mostly focused on studying the solvation structure or forecasting the theoretical redox potential of electrolytes by computing the LUMO and HOMO of each component of the electrolyte, a less-than-perfect but still-useful approximation. However, the formation of the SEI is a complicated process, which is still far from clear. Recently, molecular dynamics (MD) simulations have been widely used as a promising tool to explore complex reactions at the atomic level, especially those based on DFT.[35] The computational cost of DFT-MD or ab initio MD (AIMD) from electronic structure computations is high, preventing the simulation from reaching a sufficient time scale. Instead, a force field (FF) that is based on empirical functional forms with a trained parameter has a significant advantage in computational efficiency, which has been widely employed to simulate the battery interface in extended time and size scales. ReaxFF is one of the most popular molecular mechanic methods in battery simulation because of its unique capacity in simulating chemical reactions. Despite the success of ReaxFF,[36] challenges, such as missing FF parameters, insufficient accuracy, no explicit consideration of electron, and so forth, still impede the wide application of ReaxFF in simulating the SEI. Significant progress is being made, such as the e-ReaxFF method,[37] and so an accurate description of an electrochemical reaction is expected in the near future. Recently, Liu *et al.* proposed a hybrid *ab initio* and reactive molecular dynamics (HAIR) scheme that combines AIMD and RMD accelerating the simulation by 2 to 3 orders, while maintaining the accuracy at the DFT level.[38,39]

In this work, we investigate the initial SEI reaction of 1 M LiFSI/FDMB electrolyte with the lithium metal by using the HAIR scheme, focusing on the reduction decomposition process of this novel electrolyte and the formation mechanism of the SEI. Furthermore, X-ray photoelectron spectroscopy (XPS) analysis of the SEI based on 1.5 ns HAIR simulations was performed to reveal the detailed components, especially the inorganic part. This research provides a theoretical explanation of the reaction process of fluorinated electrolyte solvents, as well as future electrolyte design guidelines.

2. SIMULATION DETAILS

2.1. Calculation Method. The hybrid *ab initio* and reactive force field (HAIR) simulation as proposed by Liu *et al.*[38] is employed to investigate the formation of the primitive SEI in 1 M LiFSI/FDMB electrolyte at the Li metal anode. The AIMD simulation is performed using Vienna Ab initio Simulation Package (VASP) at a version of 5.4.4 with the projector augmented wave (PAW) method and a plane wave basis set. The method is DFT with generalized gradient approximations of Perdew−Burke−Ernzerhof (PBE) functional.[40] The DFT-D3 method with Becke-Jonson damping was included in the calculations.[41] The PAW method as implemented in VASP was utilized.[42] Only gamma point is considered in the calculation. The energy cut-off is set to 400 eV. A larger energy cut-off does not produce a more accurate prediction based on our benchmark calculation. The partial occupancies for each orbital are set with the first order Methfessel−Paxton scheme in the smearing width of 0.2 eV. The dipole moment corrections for the total energy are considered in the direction normal to the surface. The self-consistent electronic step is considered converged when the

https://doi.org/10.1021/acsami.1c22610
ACS Appl. Mater. Interfaces 2022, 14, 7972−7979

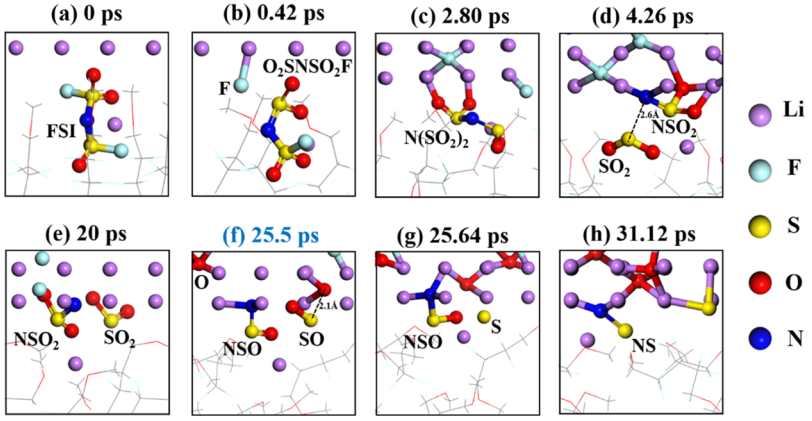

Figure 1. Sequence of FSI decompositions obtained from HAIR simulations for the FSI/FDMB mixture between 0 and 31.12 ps. (a) 0.0, (b) 0.42, (c) 2.80, (d) 4.26, (e) 20, (f) 25.5, (g) 25.64, and (h) 31.12 ps. Color code: lithium, purple; fluorine, cyan; sulfur, yellow; oxygen, red; nitrogen, blue.

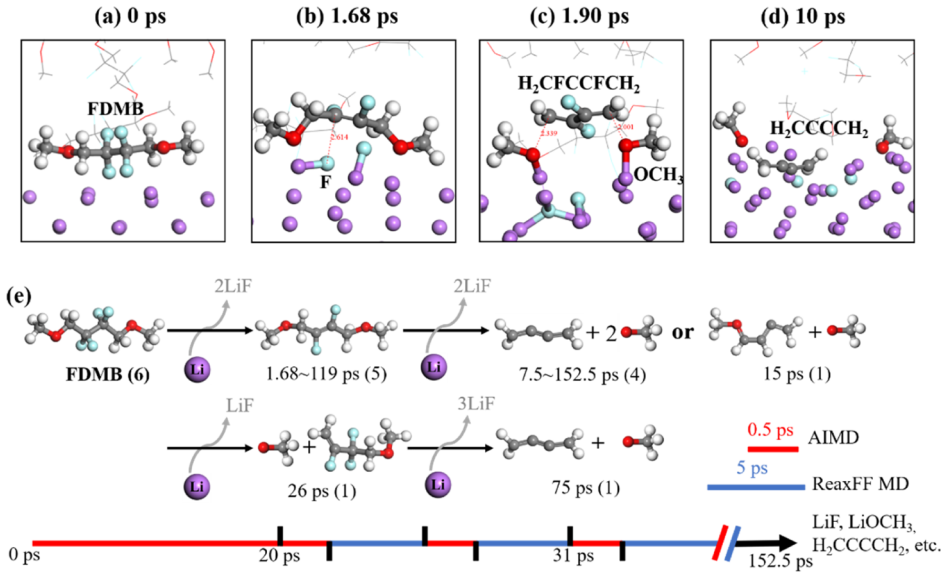

Figure 2. Reductive decomposition mechanisms of FDMB for the 1 M FSI/FDMB system. (a–d) Reaction Sequence of FDMB decompositions obtained from AIMD simulations for the FSI/FDMB mixture between 0 and 10 ps. (e) All FDMB reaction pathways obtained from HAIR simulation in 152.5 ps. The parenthesis numbers are the number of FDMB. Color code: lithium, purple; oxygen, red; carbon, gray; fluorine, cyan; sulfur, yellow; nitrogen, blue; hydrogen, white.

change of total energy and eigenvalues change between two steps are both smaller than 1×10^{-5} eV.

The ReaxFF parameters were developed based on the FF developed by Islam *et al.*,[43] which can describe Li/C/H/O/S and are specifically refined to describe several electrolytes. In our revised parameters, the N–S interaction is included, which can describe TFSI, an important salt. The FF parameters are mentioned in Supporting Information, and the details about the training set are in our previous work by Liu *et al.*[38] The ReaxFF MD (RMD) simulation is carried out using the reax/c implementation in LAMMPS using the 2008 function form. A time step of 0.25 fs is used in RMD to make sure the simulation stable by avoiding abrupt shift in forces. A canonical ensemble (*NVT*) simulation is carried out at 300 K under a Nose–Hoover thermostat with a damping parameter of 50 fs.

Before the HAIR simulations, a 20 ps AIMD simulation and a 50 ps Reax FF MD are used to determine the rationality and applicability of the model and field parameters we selected. Also, we used the structure of 20 ps AIMD for subsequent calculation. In the HAIR procedure, the AIMD and ReaxFF MD simulations are conducted alternatively using the *NVT* ensemble at 300 K, which fixes the molecule numbers (N), volume (V), and temperature (T). Moreover, the time steps for AIMD and ReaxFF were set at 1 and 0.25 fs, respectively, to guarantee good energy conservation during the HAIR simulations, while ensuring efficient convergence for collisions and smooth reactions. The HAIR simulations were conducted for 49 cycles (269.5 ps) with 10-time acceleration in the initial short-time test. Due to the slow reaction in the later stage of simulation, the product hardly changes. To reduce computational costs, we use 100 times acceleration to scale up the simulation to more than 1.5 ns.

For XPS simulation, the calculated method of core-level energy is implemented in VASP at the PBE-D3 level.[40] There are two methods to calculate the core-level shift—the initial and final state approximation, in VASP. The initial state approximation is based on Kohn–Sham's eigenvalues of the core state after self-consistent calculation of the valence charge

https://doi.org/10.1021/acsami.1c22610
ACS Appl. Mater. Interfaces 2022, 14, 7972–7979

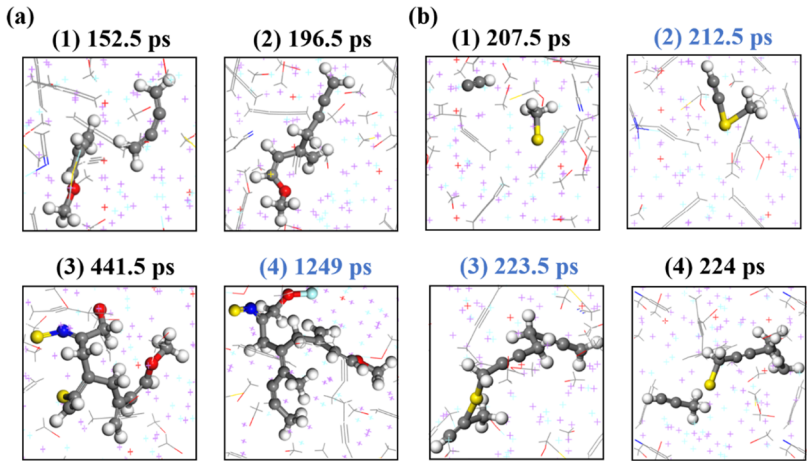

Figure 3. Sequence of polymerization reaction obtained from HAIR simulations for the 1 M LiFSI/FDMB system after 152.5 ps. (a) Snapshots for the polymer intermediate observed in simulation. (b) Role of the S radical in polymerization. The black ones are observed in AIMD, while the blue ones are observed in Reax FF MD. Color code: lithium, purple; oxygen, red; carbon, gray; fluorine, cyan; sulfur, yellow, nitrogen, blue; hydrogen, white.

density, while the final state approximation requires electrons to be removed from the core and put into the valence state.[44] Due to the reliability in reproducing the relative binding energy change as measured experimentally, we selected the initial state method to calculate the core level of the element and compared it with the corresponding binding energy in the experiment.[45] To simulate the intensity of XPS figures, a lot of AIMD trajectories, while simulating the SEI formation were used to calculate the binding energy.[46] All of the calculated binding energies are classified by the element, and the histograms of frequency distribution whose group distance is 0.1 eV are drawn according to the binding energy values, and these statistical distribution histograms were used as the raw data to fit the XPS spectrum. Peak fitting is based on peak location and structure information in trajectories.

2.2. Model of the Lithium-Electrolyte System. The Li−metal anode was represented by a 6-layer (3 × 3) supercell slab, where two of the bottom layers of the slab were fixed (Figure S1) with the most stable Li(100) surface. To achieve the desired concentrations of Li-salts in the electrolyte, we used 1 molecule LiFSI dissolved in 6 FDMB solvents to represent 1 M LiFSI/FDMB electrolyte systems. The final simulation periodic cell was 10.5 × 10.5 × 26.5 Å approximately.

3. RESULTS AND DISCUSSION

Figure 1 shows the sequence of FSI^- anion decomposition observed in HAIR simulations of the 1 M LiFSI/FDMB system. The simulation reveals that the reaction initiates from the S−F bond cleavage, consistent with previous AIMD simulations.[39,47−49] After the N−S bond breaking at 4.26 ps, all S−O bonds are decomposed sequentially by reacting with Li^0 [20−31.12 ps, as shown from Figure 1e−h], and finally, NS and S fragments and a significant amount of Li_2O formed in 31.12 ps.

In order to investigate the initial reaction process of the fluorinated ether solvent designed by Yu. et al.,[29] the reductive decomposition mechanisms of the FDMB are distinguished from AIMD reactive trajectory. As shown in Figure 2a,b, FDMB is initiated via C−F cleavage by Li^0 at around 1.68 ps and then C−O bond breaking at 1.90 ps to form $LiOCH_3$ and unsaturated carbides $H_2C{=}CF{-}CF{=}CH_2$. As the reactants are exposed to more Li^0 by diffusion, the two remaining F can be further eliminated, leaving two LiF and $H_2C{=}C{=}C{=}CH_2$.

We also summarized the reaction pathway of all FDMBs obtained from HAIR simulation in extended simulation, and the import snapshots are shown in Figure 2e. 5 out of 6 FDMBs undergo similar reaction paths as revealed from AIMD, which validates the accuracy of the HAIR simulation.[38] For the left one, FDMB, C−F bond, and C−O bond were simultaneously broken and underwent reductive reaction by Li^0 to form LiF, $LiOCH_3$, and the $H_2C{=}CF{-}CF_2{-}CH_2OCH_3$ intermediate. With the consumption of free Li^0, all C−F bonds finally cleave.

In general, ether electrolytes such as DME are relatively stable with the Li metal, but this new solvent FDMB, replacing H with F, can easily be reduced to form a large amount of LiF. Therefore, the simulation results reveal, at least, two advantages of introducing FDMB: first, the enrichment in F^- ensured that there was enough LiF phase to give the SEI with robust mechanical characteristics, comparable to those shown in prior studies with high concentration systems.[14,16,39,50−52] Second, the greater likelihood of FDMB decomposition protects the anions, which helps in maintaining the concentration of the anions required to preserve the adequate Li^+ cation.

In addition, a nanosecond scale simulation in 1 M LiFSI/FDMB is examined to more realistically depict the composition and structure of the SEI. We observed the development of several oligomer intermediates and the full formation process, as illustrated in Figure 3, contains complicated polymerization events and a variety of intermediates. During the decomposition and reduction process of FDMB, a large number of unsaturated carbides are formed. As long as the interaction is strong enough, they can continue to polymerize to form polymers. It is worth noting that we have also observed C−C polymerization with S radical insertion. As demonstrated in Figure 3b, two unsaturated carbons are united by a C−S−C bond due to the strong binding of S−C bonds. With the addition of another unsaturated carbon, H_3CCCH ultimately formed. The detailed process of these sequential oligomer reactions is shown in Figure S3.

https://doi.org/10.1021/acsami.1c22610
ACS Appl. Mater. Interfaces 2022, 14, 7972−7979

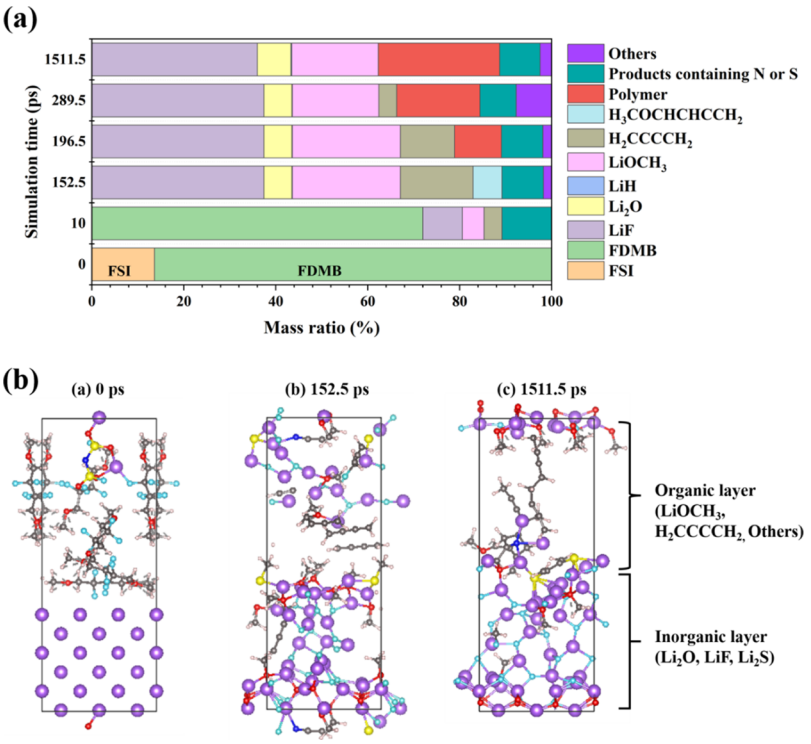

Figure 4. Composition and structure of the SEI in the 1 M LiFSI/FDMB system for MD simulation. (a) Mass ratio of main products in 1.5 ns HAIR MD simulation for 1 M LiFSI/FDMB. The selected time points indicate that 10 ps: the initial reaction of FSI and FDMB in AIMD; 152.5 ps: all of the FDMB in the system are decomposed via reacting with Li0; 196.5 ps: starting to form polymers; 289.5 ps: continue to form polymers. (b) Snapshots from MD simulation.

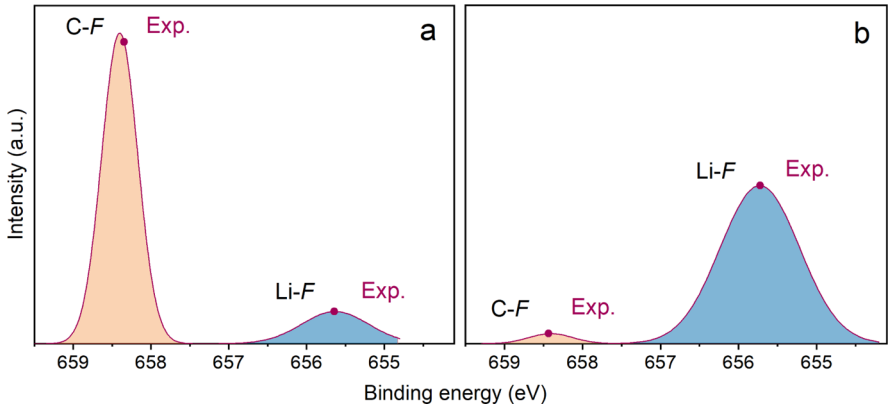

Figure 5. F 1s XPS of LiFSI with FDMB. (a) Initial stage of reaction of F 1s XPS. (b) Final stage of reaction of F 1s XPS. Experimental binding energy shift of C−F to Li−F marked with dots from Ren's work.[56]

Figure 4 depicts the changes in product distribution as a function of simulation duration, as well as the SEI atomic structure acquired after 1.5 ns HAIR simulation. As shown in Figure 4a, the S−F of the FSI^- anion was quickly cleaved to form LiF, reducing by Li^0, consistent with previous brute force AIMD simulation. The fluorinated solvent FDMB underwent a quick defluorination process in response to Li^0 diffusion, resulting in a substantial amount of LiF formation. 152.5 is a critical time point, as the defluorination reaction is essentially complete at this point, leaving enough unsaturated backbones that start polymerization. After 152.5 ps, some $H_2C{=}C{=}C{=}CH_2$ derived from FDMB as a polymer precursor will interact to form a polymer due to the presence of its unsaturated sites. At the same time, we observed that N and S radicals derived from the FSI anion also participated in the polymerization reaction under the action of the N−S bond and S−C bond (the mass ratio increases of products containing N and S from 196.5 to 298.5 ps.).

To investigate the detailed composition of the SEI obtained in 1 M LiFSI/FDMB, the time scale HAIR simulation is expanded to 1511.5 ps with 100-time acceleration (50 ps ReaxFF MD and 0.5 ps AIMD simulation.). In Figure 4b (3), the final SEI structure was formed with a composition of an inorganic inner layer (IIL) rich in LiF and an organic outer layer (OOL) composed of polymers on the surface of the lithium metal electrode.

Previous reports have shown that LiF has low electronic conductivity and high electrochemical stability, which can effectively passivate the surface of the lithium metal negative electrode, thereby protecting the lithium metal negative

https://doi.org/10.1021/acsami.1c22610
ACS Appl. Mater. Interfaces 2022, 14, 7972−7979

electrode.[25−28] In addition, the high surface of the LiF and lithium metal in the IIL can inhibit the dendrite growth of lithium. However, during the process of lithium plating/stripping, this inorganic SEI with high mechanical strength is prone to cracks. As the lithium metal electrode continues to react with the electrolyte, the SEI will also continue to grow, which may result in higher interface impedance and lower ion transport rate.[53] The OOL composed of the polymer has a certain flexibility, which can reduce or inhibit SEI cracking. In addition, it has been recently reported that the flexible polymer SEI can effectively block the penetration of lithium dendrites.[54,55] In conclusion, our results indicate that when 1 M LiFSI/FDMB is used as an electrolyte, an IIL rich in LiF and an OOL of the polymer can be formed, which can better optimize the SEI performance in terms of inhibiting the lithium dendrite and the infinite growth of the SEI. It explains the experimentally reported excellent electrochemical performance.

According to Figure 5, the analysis of the simulated XPS results proves that our results are very close to the experimental results,[29] and LiF is the main inorganic component in the SEI amorphous structure. In addition, according to Figure 5a, in the initial stage of reaction, there is little C−F bond broken in FDMB, but all S−F bonds in LiFSI are broken to form Li−F, which also indicates that the S−F bond break earlier than the C−F bond, and according to Figure 5b, the C−F bond in FDMB is basically broken, and the single Li−F bond gets stronger, which means the fluorine in Li−F mainly comes from C−F in FDMB. Meanwhile, the shift of binding energy from C−F to Li−F is 2.7 eV, as shown in Figure 5a,b, which fits well with experimental work1. After a 1.5 ns reaction when the initial frontal SEI structure was formed, the single Li−F bond is very high. XPS analysis proves that LiF is the main component of the inorganic part of the SEI.

Simulation of electrochemical reactions has drawn significant attention because of the central place of electrochemical reactions in sustainable energy.[57] It has been realized that such important effects, such as solvation effects, applied voltage (U), pH, and so forth, have to be included to reach an accurate prediction.[58−60] The advantage of our HAIR scheme is the explicit consideration of the complex and dynamically changed solvation conditions. The applied voltage is implicitly included because the work function can dynamically change in the simulation,[61] while an explicit consideration of U can be included in the near future, which provides a simulation condition closer to the *operando* experiment.

Current HAIR simulation can significantly extend the time scale of simulation at the DFT level but cannot extend the size scale due to the presence of AIMD simulation in the hybrid scheme. The strategy now is carrying out independent simulations to increase the statistics by taking advantage of the sampling average. Future development should fully replace AIMD simulation with a new implementation of advanced ReaxFF[61] or machine learning potential,[62] which can also extend the size scale in simulating electrolyte structures.

4. CONCLUSIONS

In summary, the initial reaction between the 1 M LiFSI/FDMB electrolyte and Li anode has been investigated by using a hybrid *ab initio* and reactive molecular dynamics (HAIR) scheme that can extend the simulation 10 to 100 times when compared with brute force AIMD. In more than 1.5 ns HAIR simulation, we found that both FSI^- and FDMB are reduced by Li^0 to defluorination leading to a significant amount of LiF formation. The following reactions are the S−N bond breaking in FSI^-, leading to the formation of NSO_2 and SO_2, which continue to break down via Li^0 reduction to form Li_2O, S, and NS in 31.12 ps. In this time period, no further reactions occur in FDMB. These results match the experimental results, showing that introducing FDMB provides enough F^- to create a compact inner inorganic layer (IIL) of the SEI with stable LiF and Li_2O.[29,63,64] Electronic structure calculations demonstrate that due to the strong electron-withdrawing effect of fluorine, the LUMO of the fluoro-substituted solvent is lowered and hence more readily reduced, functioning as a protective anionic salt.[21,29,65] In addition, we discovered that following defluorination, the C−O bonds of FDMB break under the influence of lithium, creating $LiOCH_3$ and H_2CCCCH_2, which is comparable to the degradation routes of DME.[66] Unsaturated organics, such as H_2CCCCH_2, begin to polymerize around 196.5 ps, and two unsaturated carbon organics can polymerize when S and unsaturated carbon contact. Together with $LiOCH_3$, these oligomers form the OOL of the SEI. During the electrodeposition process, the SEI is influenced by pressure and stress.[67−70] The presence of oligomers improves SEI's viscoelasticity, lowering the risk of mechanical fracture. The detailed link between the polymer structure and SEI properties will be investigated in future work.

■ ASSOCIATED CONTENT

Supporting Information

The Supporting Information is available free of charge at https://pubs.acs.org/doi/10.1021/acsami.1c22610.

Details and snapshots of the decomposition pathways of all FDMB; details of polymerization reaction from long-time HAIR trajectory; molecular orbital of HOMO and LUMO of FDMB and LiFSI; detail description of the electrolyte models; ReaxFF parameters, and HAIR simulation example files (PDF)

■ AUTHOR INFORMATION

Corresponding Author

Tao Cheng − *Institute of Functional Nano and Soft Materials (FUNSOM), Soochow University, Suzhou 215123, China;* orcid.org/0000-0003-4830-177X; Email: tcheng@suda.edu.cn

Authors

Peiping Yu − *Institute of Functional Nano and Soft Materials (FUNSOM), Soochow University, Suzhou 215123, China*

Qintao Sun − *Institute of Functional Nano and Soft Materials (FUNSOM), Soochow University, Suzhou 215123, China*

Yue Liu − *Institute of Functional Nano and Soft Materials (FUNSOM), Soochow University, Suzhou 215123, China*

Bingyun Ma − *Institute of Functional Nano and Soft Materials (FUNSOM), Soochow University, Suzhou 215123, China*

Hao Yang − *Institute of Functional Nano and Soft Materials (FUNSOM), Soochow University, Suzhou 215123, China;* orcid.org/0000-0002-8241-6231

Miao Xie − *Institute of Functional Nano and Soft Materials (FUNSOM), Soochow University, Suzhou 215123, China;* orcid.org/0000-0002-9797-1449

Complete contact information is available at:

https://pubs.acs.org/10.1021/acsami.1c22610

Author Contributions

†These authors contribute equally.

Notes

The authors declare no competing financial interest.

■ ACKNOWLEDGMENTS

T.C. thanks the support from Suzhou Key Laboratory of Functional Nano & Soft Materials, Collaborative Innovation Center of Suzhou Nano Science & Technology, the Priority Academic Program Development of Jiangsu Higher Education Institutions (PAPD), the 111 Project, Joint International Research Laboratory of Carbon-Based Functional Materials and Devices, the National Natural Science Foundation of China (21903058 and 22173066), the Natural Science Foundation of Jiangsu Higher Education Institutions (SBK20190810), and the Jiangsu Province High-Level Talents (JNHB-106).

■ REFERENCES

(1) Lin, D.; Liu, Y.; Cui, Y. Reviving the Lithium Metal Anode for High-Energy Batteries. *Nat. Nanotechnol.* **2017**, *12*, 194−206.
(2) Armand, M.; Tarascon, J.-M. Building Better Batteries. *Nature* **2008**, *451*, 652−657.
(3) Xu, W.; Wang, J.; Ding, F.; Chen, X.; Nasybulin, E.; Zhang, Y.; Zhang, J.-G. Lithium Metal Anodes for Rechargeable Batteries. *Energy Environ. Sci.* **2014**, *7*, 513−537.
(4) Qian, J.; Henderson, W. A.; Xu, W.; Bhattacharya, P.; Engelhard, M.; Borodin, O.; Zhang, J.-G. High Rate and Stable Cycling of Lithium Metal Anode. *Nat. Commun.* **2015**, *6*, 6362.
(5) Cheng, X.-B.; Zhang, R.; Zhao, C.-Z.; Wei, F.; Zhang, J.-G.; Zhang, Q. A Review of Solid Electrolyte Interphases on Lithium Metal Anode. *Adv. Sci.* **2016**, *3*, 1500213.
(6) Goodenough, J. B.; Kim, Y. Challenges for Rechargeable Li Batteries. *Chem. Mater.* **2009**, *22*, 587−603.
(7) Peled, E. The Electrochemical Behavior of Alkali and Alkaline Earth Metals in Nonaqueous Battery Systems—The Solid Electrolyte Interphase Model. *J. Electroanal. Chem.* **1979**, *126*, 2047.
(8) Yamada, Y.; Furukawa, K.; Sodeyama, K.; Kikuchi, K.; Yaegashi, M.; Tateyama, Y.; Yamada, A. Unusual Stability of Acetonitrile-based Superconcentrated Electrolytes for Fast-Charging Lithium-Ion Batteries. *J. Am. Chem. Soc.* **2014**, *136*, 5039−5046.
(9) Wang, J.; Yamada, Y.; Sodeyama, K.; Chiang, C. H.; Tateyama, Y.; Yamada, A. Superconcentrated Electrolytes for a High-Voltage Lithium-Ion Battery. *Nat. Commun.* **2016**, *7*, 12032.
(10) Yoshida, K.; Nakamura, M.; Kazue, Y.; Tachikawa, N.; Tsuzuki, S.; Seki, S.; Dokko, K.; Watanabe, M. Oxidative-Stability Enhancement and Charge Transport Mechanism in Glyme-Lithium Salt Equimolar Complexes. *J. Am. Chem. Soc.* **2011**, *133*, 13121−13129.
(11) Yamada, Y.; Wang, J.; Ko, S.; Watanabe, E.; Yamada, A. Advances and Issues in Developing Salt-Concentrated Battery Electrolytes. *Nat. Energy* **2019**, *4*, 269−280.
(12) Wang, J.; Yamada, Y.; Sodeyama, K.; Watanabe, E.; Takada, K.; Tateyama, Y.; Yamada, A. Fire-Extinguishing Organic Electrolytes for Safe Batteries. *Nat. Energy* **2017**, *3*, 22−29.
(13) Zheng, J.; Lochala, J. A.; Kwok, A.; Deng, Z. D.; Xiao, J. Research Progress towards Understanding the Unique Interfaces between Concentrated Electrolytes and Electrodes for Energy Storage Applications. *Adv. Sci.* **2017**, *4*, 1700032.
(14) Matsumoto, K.; Inoue, K.; Nakahara, K.; Yuge, R.; Noguchi, T.; Utsugi, K. Suppression of Aluminum Corrosion by using High Concentration LiTFSI Electrolyte. *J. Power Sources* **2013**, *231*, 234−238.
(15) Takada, K.; Yamada, Y.; Yamada, A. Optimized Nonflammable Concentrated Electrolytes by Introducing a Low-Dielectric Diluent. *ACS Appl. Mater. Interfaces* **2019**, *11*, 35770−35776.
(16) Wu, C.; Zhou, Y.; Zhu, X. L.; Zhan, M. Z.; Yang, H. X.; Qian, J. F. Research Progress on High Concentration Electrolytes for Li Metal Batteries. *Acta Phys.-Chim. Sin.* **2021**, *37*, 2008044−2008050.
(17) Xu, K. Nonaqueous Liquid Electrolytes for Lithium-Based Rechargeable Batteries. *Chem. Rev.* **2004**, *104*, 4303−4418.
(18) Croce, F.; Appetecchi, G. B.; Persi, L.; Scrosati, B. Nanocomposite Polymer Electrolytes for Lithium Batteries. *Nature* **1998**, *394*, 456−458.
(19) Aurbach, D. A Short Review of Failure Mechanisms of Lithium Metal and Lithiated Graphite Anodes in Liquid Electrolyte Solutions. *Solid State Ionics* **2002**, *148*, 405−416.
(20) Jiao, S.; Ren, X.; Cao, R.; Engelhard, M. H.; Liu, Y.; Hu, D.; Mei, D.; Zheng, J.; Zhao, W.; Li, Q.; Liu, N.; Adams, B. D.; Ma, C.; Liu, J.; Zhang, J.-G.; Xu, W. Stable Cycling of High-Voltage Lithium Metal Batteries in Ether Electrolytes. *Nat. Energy* **2018**, *3*, 739−746.
(21) Jaumaux, P.; Wu, J. R.; Shanmukaraj, D.; Wang, Y. Z.; Zhou, D.; Sun, B.; Kang, F. Y.; Li, B. H.; Armand, M.; Wang, G. X. Non-Flammable Liquid and Quasi-Solid Electrolytes toward Highly-Safe Alkali Metal-Based Batteries. *Adv. Funct. Mater.* **2021**, *31*, 2008644.
(22) Cho, S.-J.; Yu, D.-E.; Pollard, T. P.; Moon, H.; Jang, M.; Borodin, O.; Lee, S.-Y. Nonflammable Lithium Metal Full Cells with Ultra-high Energy Density Based on Coordinated Carbonate Electrolytes. *iScience* **2020**, *23*, 100844.
(23) Cheng, X.-B.; Zhang, R.; Zhao, C.-Z.; Zhang, Q. Toward Safe Lithium Metal Anode in Rechargeable Batteries: A Review. *Chem. Rev.* **2017**, *117*, 10403−10473.
(24) Nagasubramanian, G.; Fenton, K. Reducing Li-Ion Safety Hazards through use of Non-Flammable Solvents and Recent Work at Sandia National Laboratories. *Electrochim. Acta* **2013**, *101*, 3−10.
(25) Lu, Y.; Tu, Z.; Archer, L. A. Stable Lithium Electrodeposition in Liquid and Nanoporous Solid Electrolytes. *Nat. Mater.* **2014**, *13*, 961−969.
(26) Fan, X.; Ji, X.; Han, F.; Yue, J.; Chen, J.; Chen, L.; Deng, T.; Jiang, J.; Wang, C. Fluorinated Solid Electrolyte Interphase Enables Highly Reversible Solid-State Li Metal Battery. *Sci. Adv.* **2018**, *4*, No. eaau9245.
(27) Zhao, J.; Liao, L.; Shi, F.; Lei, T.; Chen, G.; Pei, A.; Sun, J.; Yan, K.; Zhou, G.; Xie, J.; Liu, C.; Li, Y.; Liang, Z.; Bao, Z.; Cui, Y. Surface Fluorination of Reactive Battery Anode Materials for Enhanced Stability. *J. Am. Chem. Soc.* **2017**, *139*, 11550−11558.
(28) Huang, W.; Wang, H.; Boyle, D. T.; Li, Y.; Cui, Y. Resolving Nanoscopic and Mesoscopic Heterogeneity of Fluorinated Species in Battery Solid-Electrolyte Interphases by Cryogenic Electron Microscopy. *ACS Energy Lett.* **2020**, *5*, 1128−1135.
(29) Yu, Z.; Wang, H.; Kong, X.; Huang, W.; Tsao, Y.; Mackanic, D. G.; Wang, K.; Wang, X.; Huang, W.; Choudhury, S.; Zheng, Y.; Amanchukwu, C. V.; Hung, S. T.; Ma, Y.; Lomeli, E. G.; Qin, J.; Cui, Y.; Bao, Z. Molecular design for electrolyte solvents enabling energy-dense and long-cycling lithium metal batteries. *Nat. Energy* **2020**, *5*, 526−533.
(30) Yuan, Q.; Yang, H.; Xie, M.; Cheng, T. Theoretical Research on the Electroreduction of Carbon Dioxide. *Acta Phys.-Chim. Sin.* **2020**, *37*, 2010040.
(31) Long, J.; Chen, S.; Zhang, Y.; Guo, C.; Fu, X.; Deng, D.; Xiao, J. Direct Electrochemical Ammonia Synthesis from Nitric Oxide. *Angew. Chem., Int. Ed. Engl.* **2020**, *59*, 9711−9718.
(32) Kresse, G.; Hafner, J. Ab initio molecular dynamics for liquid metals. *Phys. Rev. B: Condens. Matter Mater. Phys.* **1993**, *47*, 558−561.
(33) Delp, S. A.; Borodin, O.; Olguin, M.; Eisner, C. G.; Allen, J. L.; Jow, T. R. Importance of Reduction and Oxidation Stability of High Voltage Electrolytes and Additives. *Electrochim. Acta* **2016**, *209*, 498−510.
(34) Wang, Q.; Yao, Z.; Zhao, C.; Verhallen, T.; Tabor, D. P.; Liu, M.; Ooms, F.; Kang, F.; Aspuru-Guzik, A.; Hu, Y.-S.; Wagemaker, M.; Li, B. Interface Chemistry of an Amide Electrolyte for Highly Reversible Lithium Metal Batteries. *Nat. Commun.* **2020**, *11*, 4188.
(35) Xie, M.; Wu, Y.; Liu, Y.; Yu, P. P.; Jia, R.; Goddard, W. A.; Cheng, T. Pathway of In Situ Polymerization of 1,3-Dioxolane in

LiPF6 Electrolyte on Li Metal Anode. *Mater. Today Energy* **2021**, *21*, 100730.
(36) Senftle, T. P.; Hong, S.; Islam, M. M.; Kylasa, S. B.; Zheng, Y.; Shin, Y. K.; Junkermeier, C.; Engel-Herbert, R.; Janik, M. J.; Aktulga, H. M.; Verstraelen, T.; Grama, A.; van Duin, A. C. T. The ReaxFF Reactive Force-Field: Development, Applications and Future Directions. *npj Comput. Mater.* **2016**, *2*, 1.
(37) Evangelisti, B.; Fichthorn, K. A.; van Duin, A. C. T. Development and Initial Applications of an e-ReaxFF Description of Ag Nanoclusters. *J. Chem. Phys.* **2020**, *153*, 104106.
(38) Liu, Y.; Yu, P.; Wu, Y.; Yang, H.; Xie, M.; Huai, L.; Goddard, W. A.; Cheng, T. The DFT-ReaxFF Hybrid Reactive Dynamics Method with Application to the Reductive Decomposition Reaction of the TFSI and DOL Electrolyte at a Lithium-Metal Anode Surface. *J. Phys. Chem. Lett.* **2021**, *12*, 1300−1306.
(39) Liu, Y.; Sun, Q.; Yu, P.; Wu, Y.; Xu, L.; Yang, H.; Xie, M.; Cheng, T.; Goddard, W. A. Effects of High and Low Salt Concentrations in Electrolytes at Lithium-Metal Anode Surfaces Using DFT-ReaxFF Hybrid Molecular Dynamics Method. *J. Phys. Chem. Lett.* **2021**, *12*, 2922−2929.
(40) Perdew, J. P.; Burke, K.; Ernzerhof, M. Generalized Gradient Approximation Made Simple. *Phys. Rev. Lett.* **1996**, *77*, 3865−3868.
(41) Grimme, S.; Ehrlich, S.; Goerigk, L. Effect of the damping function in dispersion corrected density functional theory. *J. Comput. Chem.* **2011**, *32*, 1456−1465.
(42) Kresse, G.; Joubert, D. From ultrasoft pseudopotentials to the projector augmented-wave method. *Phys. Rev. B* **1999**, *59*, 1758−1775.
(43) Islam, M. M.; Bryantsev, V. S.; van Duin, A. C. T. ReaxFF Reactive Force Field Simulations on the Influence of Teflon on Electrolyte Decomposition during Li/SWCNT Anode Discharge in Lithium-Sulfur Batteries. *J. Electroanal. Chem.* **2014**, *161*, E3009−E3014.
(44) Köhler, L.; Kresse, G. Density functional study of CO on Rh(111). *Phys. Rev. B* **2004**, *70*, 165405.
(45) Yang, H.; Negreiros, F. R.; Sun, Q.; Xie, M.; Sementa, L.; Stener, M.; Ye, Y.; Fortunelli, A.; Goddard, W. A., 3rd; Cheng, T. Predictions of Chemical Shifts for Reactive Intermediates in CO2 Reduction under Operando Conditions. *ACS Appl. Mater. Interfaces* **2021**, *13*, 31554−31560.
(46) Qian, J.; Baskin, A.; Liu, Z.; Prendergast, D.; Crumlin, E. J. Addressing the Sensitivity of Signals from Solid/Liquid Ambient Pressure XPS (APXPS) Measurement. *J. Chem. Phys.* **2020**, *153*, 044709.
(47) Zhang, H.; Shen, C.; Huang, Y.; Liu, Z. Spontaneously Formation of SEI Layers on Lithium Metal from LiFSI/DME and LiTFSI/DME Electrolytes. *Appl. Surf. Sci.* **2021**, *537*, 147983.
(48) Galvez-Aranda, D. E.; Seminario, J. M. Li-Metal Anode in Dilute Electrolyte LiFSI/TMP: Electrochemical Stability Using Ab Initio Molecular Dynamics. *J. Phys. Chem. C* **2020**, *124*, 21919−21934.
(49) Eshetu, G. G.; Judez, X.; Li, C.; Martinez-Ibañez, M.; Gracia, I.; Bondarchuk, O.; Carrasco, J.; Rodriguez-Martinez, L. M.; Zhang, H.; Armand, M. Ultrahigh Performance All Solid-State Lithium Sulfur Batteries: Salt Anion's Chemistry-Induced Anomalous Synergistic Effect. *J. Am. Chem. Soc.* **2018**, *140*, 9921−9933.
(50) Chen, S.; Zheng, J.; Mei, D.; Han, K. S.; Engelhard, M. H.; Zhao, W.; Xu, W.; Liu, J.; Zhang, J. G. High-Voltage Lithium-Metal Batteries Enabled by Localized High-Concentration Electrolytes. *Adv. Mater.* **2018**, *30*, 1706102.
(51) Zhang, B.; Lin, Z.; Chen, H.; Wang, L.-W.; Pan, F. The Stability and Reaction Mechanism of a LiF/Electrolyte Interface: Insight from Density Functional Theory. *J. Mater. Chem. A* **2020**, *8*, 2613−2617.
(52) Han, H.-B.; Zhou, S.-S.; Zhang, D.-J.; Feng, S.-W.; Li, L.-F.; Liu, K.; Feng, W.-F.; Nie, J.; Li, H.; Huang, X.-J. Lithium Bis(fluorosulfonyl)imide (LiFSI) as Conducting Salt for Nonaqueous Liquid Electrolytes for Lithium-Ion Batteries: Physicochemical and Electrochemical Properties. *J. Power Sources* **2011**, *196*, 3623−3632.
(53) Hao, F.; Verma, A.; Mukherjee, P. P. Mechanistic Insight into Dendrite−SEI Interactions for Lithium Metal Electrodes. *J. Mater. Chem. A* **2018**, *6*, 19664−19671.
(54) Zhang, C.; Jin, T.; Cheng, G.; Yuan, S.; Sun, Z.; Li, N.-W.; Yu, L.; Ding, S. Functional Polymers in Electrolyte Optimization and Interphase Design for Lithium Metal Anodes. *J. Mater. Chem. A* **2021**, *9*, 13388.
(55) Monroe, C.; Newman, J. The Impact of Elastic Deformation on Deposition Kinetics at Lithium/Polymer Interfaces. *J. Electroanal. Chem.* **2005**, *152*, A396−A404.
(56) Ren, X.; Gao, P.; Zou, L.; Jiao, S.; Cao, X.; Zhang, X.; Jia, H.; Engelhard, M. H.; Matthews, B. E.; Wu, H.; Lee, H.; Niu, C.; Wang, C.; Arey, B. W.; Xiao, J.; Liu, J.; Zhang, J.-G.; Xu, W. Role of Inner Solvation Sheath within Salt-Solvent Complexes in Tailoring Electrode/Electrolyte Interphases for Lithium Metal Batteries. *Proc. Natl. Acad. Sci. U.S.A.* **2020**, *117*, 28603−28613.
(57) He, Q.; Yu, B.; Li, Z.; Zhao, Y. Density Functional Theory for Battery Materials. *Energy Environ. Mater.* **2019**, *2*, 264−279.
(58) Zhao, X.; Liu, Y. Origin of Selective Production of Hydrogen Peroxide by Electrochemical Oxygen Reduction. *J. Am. Chem. Soc.* **2021**, *143* (25), 9423−9428.
(59) Xiao, H.; Cheng, T.; Goddard, W. A.; Sundararaman, R. Mechanistic Explanation of the pH Dependence and Onset Potentials for Hydrocarbon Products from Electrochemical Reduction of CO on Cu (111). *J. Am. Chem. Soc.* **2016**, *138*, 483−486.
(60) Cheng, T.; Xiao, H.; Goddard, W. A. Free-Energy Barriers and Reaction Mechanisms for the Electrochemical Reduction of CO on the Cu(100) Surface, Including Multiple Layers of Explicit Solvent at pH 0. *J. Phys. Chem. Lett.* **2015**, *6*, 4767−4773.
(61) Liu, Y.; Sun, Q.; Yu, P.; Ma, B.; Yang, H.; Zhang, J.; Xie, M.; Cheng, T. In situ formation of circular and branched oligomers in a localized high concentration electrolyte at the lithium-metal solid electrolyte interphase: a hybrid ab initio and reactive molecular dynamics study. *J. Mater. Chem. A* **2022**, *10*, 632−639.
(62) Yanxon, H.; Zagaceta, D.; Tang, B.; Matteson, D. S.; Zhu, Q. PyXtal_FF: A Python Library for Automated Force Field Generation. *Mach. Learn.: Sci. Technol.* **2020**, *2*, 027001.
(63) Wang, H.; Yu, Z.; Kong, X.; Huang, W.; Zhang, Z.; Mackanic, D. G.; Huang, X.; Qin, J.; Bao, Z.; Cui, Y. Dual-Solvent Li-Ion Solvation Enables High-Performance Li-Metal Batteries. *Adv. Mater.* **2021**, *33*, 2008619.
(64) Wang, H.; Huang, W.; Yu, Z.; Huang, W.; Xu, R.; Zhang, Z.; Bao, Z.; Cui, Y. Efficient Lithium Metal Cycling over a Wide Range of Pressures from an Anion-Derived Solid-Electrolyte Interphase Framework. *ACS Energy Lett.* **2021**, *6*, 816−825.
(65) Hua, G.; Fan, Y.; Zhang, Q. Application of Computational Simulation on the Study of Lithium Metal Anodes. *Acta Phys.-Chim. Sin.* **2020**, *37*, 2008089−2008090.
(66) Camacho-Forero, L. E.; Balbuena, P. B. Elucidating Electrolyte Decomposition under Electron-Rich Environments at the Lithium-Metal Anode. *Phys. Chem. Chem. Phys.* **2017**, *19*, 30861−30873.
(67) Zhao, Q.; Stalin, S.; Archer, L. A. Stabilizing Metal Battery Anodes through the Design of Solid Electrolyte Interphases. *Joule* **2021**, *5*, 1119−1142.
(68) Wang, G.; Chen, C.; Chen, Y.; Kang, X.; Yang, C.; Wang, F.; Liu, Y.; Xiong, X. Self-Stabilized and Strongly Adhesive Supramolecular Polymer Protective Layer Enables Ultrahigh-Rate and Large-Capacity Lithium-Metal Anode. *Angew. Chem., Int. Ed.* **2020**, *59*, 2055−2060.
(69) Wei, S.; Cheng, Z.; Nath, P.; Tikekar, M. D.; Li, G.; Archer, L. A. Stabilizing Electrochemical Interfaces in Viscoelastic Liquid Electrolytes. *Sci. Adv.* **2018**, *4*, No. eaao6243.
(70) Liu, K.; Pei, A.; Lee, H. R.; Kong, B.; Liu, N.; Lin, D.; Liu, Y.; Liu, C.; Hsu, P.-c.; Bao, Z.; Cui, Y. Lithium Metal Anodes with an Adaptive "Solid-Liquid" Interfacial Protective Layer. *J. Am. Chem. Soc.* **2017**, *139*, 4815−4820.

https://doi.org/10.1021/acsami.1c22610
ACS Appl. Mater. Interfaces 2022, 14, 7972−7979